IEEE Access
Multidisciplinary ⋮ Rapid Review ⋮ Open Access Journal

Received 30 June 2022, accepted 18 July 2022, date of publication 21 July 2022, date of current version 27 July 2022.

Digital Object Identifier 10.1109/ACCESS.2022.3193134

RESEARCH ARTICLE

Analysis and Suppression of Oscillation in Traction Network-EMUs Coupling System Under the Condition of Rising Pantograph

XUESONG ZHOU[1], YIFAN HU[1], YOUJIE MA[1], AND YU TIAN[2]

[1]Tianjin Key Laboratory for Control Theory and Applications in Complicated Industry Systems, School of Electrical and Electronic Engineering, Tianjin University of Technology, Tianjin 300384, China
[2]Manufacturing Technology Center, CRRC TANGSHAN Company Ltd., Tangshan 064000, China

Corresponding author: Yifan Hu (huyifan118@126.com)

This work was supported in part by the National Natural Science Foundation of China under Grant 51877152, and in part by the Tianjin Research Innovation Project for Postgraduate Students under Grant 2021YJSS090.

ABSTRACT Low frequency oscillation (LFO) incidents may occur in coupled system composed of electric multiple units (EMUs) and traction network, which threaten the safety and stability of EMUs and traction power supply system. In order to solve this problem, a virtual impedance with band-pass filter link control strategy is proposed for the four quadrant converters (4QCs) of EMU. First, the impedance models of coupled system under the background of LFO are established based on the impedance matching. Next, this paper defines the worst scenario for coupled system, combined with the Nyquist curve and forbidden region criterion (FRC). The impact of the grid-side and EMU-side circuit parameters on system stability is analyzed. The proposed control strategy adjusts the input impedance of the EMUs equivalently by virtual impedance to meet FRC. Band-pass filter (BPF) is used to select a specific band to apply virtual impedance. This avoids passive impact on the dynamic performance of other frequency band. The parameters of the virtual impedance and BPF are designed according to the FRC and engineering requirements. The simulation results verify the effectiveness of the proposed control strategy for oscillation suppression. Finally, the coupled system model is built on the basis of hardware-in-the-loop experimental platform. The experimental results show that the proposed method can be used to suppress oscillations.

INDEX TERMS Long series EMUs-traction network system, impedance matching, forbidden region criterion, band-pass filter, virtual impedance control.

I. INTRODUCTION

In recent years, rail transit has developed significantly in China. EMU is becoming the preferred mode of transportation for the public. Chinese standard EMU trains named ''Fuxing'' represents a spectrum of EMUs. They will develop in the direction of lightweight, main and auxiliary integration [1]. Source-network-train-storage integrated system has been proposed for electric railways. Among the integrated system, it is necessary to ensure the stability of traction network-EMUs coupling system. It is the most basic and important component of the traction power supply system (TPSS) [2]. However, it has been recorded that LFO accidents have occurred many times in the coupled system [3]. LFO seriously threatens the normal railway operation order and poses threat to the stability of the EMUs.

The traction network-EMUs coupling system can be regarded as a cascaded system composed of weak grid and converters [4]. Scholars have adopted different methods to analyze system stability, such as impedance analysis method in frequency-domain [5] and eigenvalue analysis method in time-domain [6]-[7]. For the impact factors, [8] proposes that it is more likely to occur in the state of rising pantograph than the state of fully operating; In [9], the influence of traction network parameters on the system stability are analyzed. When the inductance of the network-side increases, the

The associate editor coordinating the review of this manuscript and approving it for publication was Yuh-Shyan Hwang.

system is more likely to occur LFO incidents. It is manifested as the farther the distance between power supply station and EMUs, the more likely the system coupling LFO occurs; Short-series EMUs are taken as the analysis objects in [10]. The maximum number of EMUs allowed is six when they are lightly loaded at a closer distance simultaneously. However, since the input impedance model may be different, the conclusions on the impact of EMU number may not be applicable to the long-series EMUs [11] or vehicles which are fully operating. In [6], the eigenvalue analysis method is adopted. Combining the actual EMU design requirements with damping calculation, a basis for its subsequent passive controller design is provided. The impedance models of vehicle-traction network are established and analyzed in [4]. It is concluded that impedance mismatch is the main cause of instability. But the specific affecting factors are not stated.

For the improvement of cascaded system stability, most of the existing literatures studied from two perspectives, adjusting the relevant parameters [12]-[13] and imposing control [14]. Since the parameters are closely coupled in the actual system, the adjustment of the parameters will affect other settings and may require a large amount of engineering. So the applied control approach may be relatively easy to implement [15]-[16]. Specific control strategies can be classified as passive control [17], nonlinear control [18] and active control strategies [19]. In [20], based on the installation of static synchronous compensator (STATCOM) [21], it is proposed that the adoption of active power filtering devices can better suppress the occurrence of LFO and enhance system stability. However, the improvements for the network side often have the drawback of huge engineering effort. So the researchers prefer to improve control strategy for traction converters of EMUs, especially for the newly manufactured EMUs of the host plant. [22] adopts passivity based control to ensure the global stability of the system. Active disturbance rejection control (ADRC) is adopted in [23]. It uses the state feedback of the state observer to replace the output feedback of the original controller and achieves better control effect. Compared with the other control methods such as proportional integral control, It is more effective in suppressing LFO. By adopting this method, the conflict between overshoot and rapidity is resolved. However, ADRC strategy may be difficult to rectify due to the number of parameters it requires, which is not conducive to parametric design. A virtual inertia control strategy with adaptive sliding mode observer to suppress the occurrence of LFO is reported by the authors in [24]. But the design of its state observer parameters is vulnerable to the actual system error. A notch filter is designed to suppress LFO in [25], which is essentially an active control strategy. Reference [19] adopts proportional-derivative control strategy. It can equivalently changes vehicle input impedance to make the system satisfy the corresponding steady-state criterion. But the dynamic performance near the cut-off frequency of the proposed low-pass filter will be affected, and the performance of EMU may be affected while suppressing LFO.

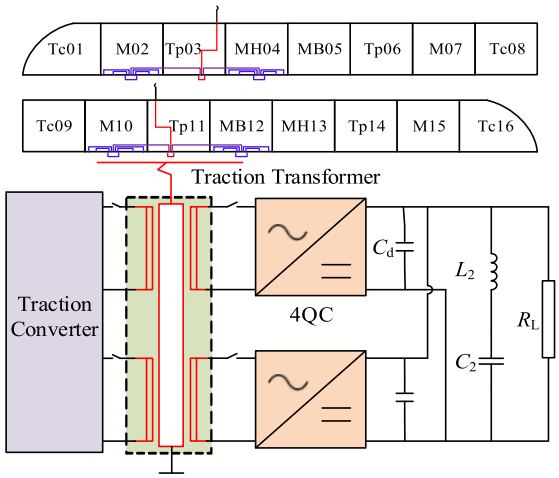

FIGURE 1. Main circuit structure of traction unit.

Considering the deficiencies in the above researches, this paper proposes a virtual resistive control strategy with the introduction of band-pass filtering link for 4QC of EMUs. The rest of this paper is organized as follows. In Section II, the structure of traction converter and existing 4QC control strategy are showed. In Section III, the input impedance model of EMU and the output impedance of the traction network are established. Based on the Nyquist curve of the open-loop transfer function and FRC [26], the impact of various electrical parameters, EMU operation states and other factors on the coupled system stability is analyzed. In Section IV, control strategy is proposed and the influence of virtual impedance and band-pass filter on system dynamic performance and stability is analyzed. And the corresponding parameters are designed. In Section V, a simulation model of the coupled system is built, and the simulation and experiment verify the correctness of the analysis results and the effectiveness of the proposed control strategy.

II. INTRODUCTION OF EMU TRACTION CONVERTER

A. STRUCTURE OF EMU TRACTION UNITS

Fig. 1 shows the main circuit structure of EMU traction units. It consists of the traction transformer secondary side, traction converters, traction motors and traction control unit (TCU). Among them, the traction converter consists of two parallel duplicated 4QCs, intermediate DC link, traction inverters and towing mode devices.

The traction system of the ''Fuxing'' long-series EMU consists of four traction units, each consisting of two motor units and two trailer units, and the four traction units adopt a symmetrical design. The load is composed of the traction inverters and auxiliary converters. In Fig. 1, C_d is the DC-side support capacitor of the traction converter, L_2 and C_2 are the DC-side second resonance circuit filter inductor and capacitor respectively. When traction converters begin to operate or only the auxiliary converter is fully operated, the load

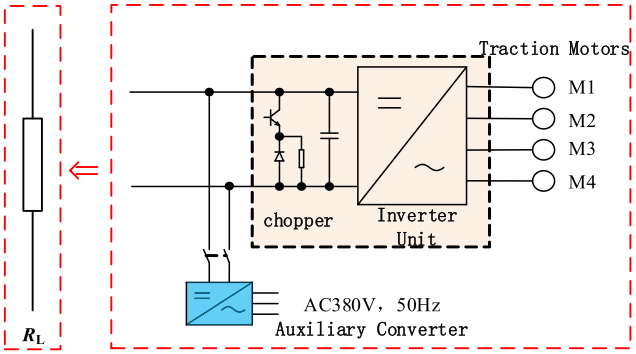

FIGURE 2. Schematic diagram of load equivalence.

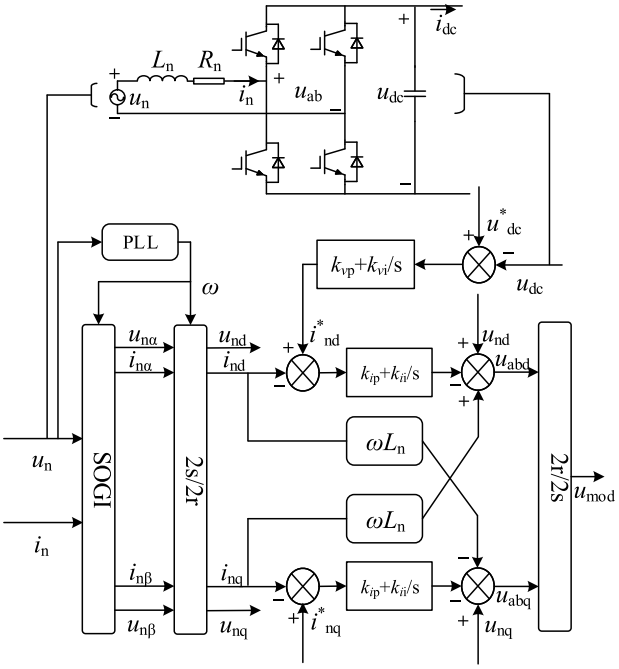

FIGURE 3. Diagram of dq decoupling current control for 4QC.

can be equated to the form of resistance R_L. The equivalent schematic diagram is shown in Fig. 2.

B. EXSITING CONTROL STRATEGY

4QC mostly adopts instantaneous current control strategy or decoupling current control strategy, among which dq decoupling current control can meet the needs of higher power loads.

Fig. 3 shows the control strategy diagram, where u_n is the AC-side voltage of 4QC; i_n is the AC-side current of 4QC; L_n is the equivalent leakage inductance of the traction transformer; R_n is the equivalent leakage resistance of the traction transformer; u_{nd} and u_{nq} are the d-axis and q-axis components of u_n; i_{nd} and i_{nq} are the d-axis and q-axis components of i_n; u^*_{dc} is the DC-side reference voltage; i^*_{nd} and i^*_{nq} denote the d-axis and q-axis reference current, respectively; k_{vp} and k_{vi} denote the outer-loop proportional and integral coefficients of PI controller; k_{ip} and k_{ii} denote the proportional

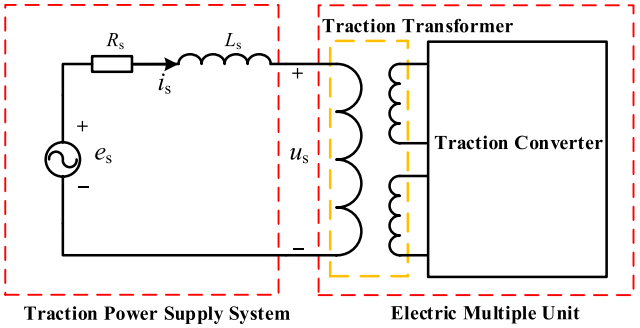

FIGURE 4. Schematic diagram of Traction- EMUs coupling.

and integral coefficients of inner-loop PI controller; u_{mod} is the generated voltage modulation signal; i_{dc} is the output current of 4QC. In this paper, 4QC adopts the dq decoupling current control based on Second-Order General Integrator (SOGI)-Phase Locked Loop (PLL). u_n and i_n can be transformed into dq frame components by SOGI-PLL and 2s/2r transformation.

III. IMPEDANCE MODELING AND STABILITY ANALYSIS

A. OUTPUT IMPEDANCE MODEL OF NETWORK

For the LFO of the coupled system, the traction network output impedance model can be equated to a series resistance-inductance circuit of the form $Z_s = R_s + j\omega L_s$ [15]. Z_s is the traction network equivalent output impedance, R_s is the traction network equivalent resistance, and L_s is the traction network equivalent inductance. Fig. 4 shows the traction network-EMU coupling model, where u_s is the voltage at the coupling point and i_s is the current through the coupling point. It shows that the degree of dd-axis impedance matching in the system open-loop transfer function has the most obvious effect on the system stability in [19]. The feasibility of researching dd-axis impedance matching for high power factor cascade systems to achieve stability analysis of AC systems has been clarified in [27]. Therefore, this paper focuses on analyzing the effects of different factors on the dd-axis component based on the system open-loop transfer function. The output impedance dd-axis component $Z_{sdd}(s)$ of the traction network side is shown in (1).

$$Z_{sdd}(s) = R_s + sL_s \tag{1}$$

B. INPUT IMPEDANCE MODEL OF EMU

To establish the input impedance model of 4QC, the mathematical expression can be obtained according to Fig. 3, combined with the Laplace transformation as

$$\begin{cases} u_n = (j\omega L_n + R_n)i_n + u_{ab} \\ u_{nd}(s) = (sL_n + R_n)i_{nd}(s) + u_{abd}(s) - \omega L_n i_{nq}(s) \\ u_{nq}(s) = (sL_n + R_n)i_{nq}(s) + u_{abq}(s) + \omega L_n i_{nd}(s) \end{cases} \tag{2}$$

where u_{ab} is the input voltage of the network side rectifier, u_{abd} and u_{abq} are the d and q axis components of u_{ab}. Since

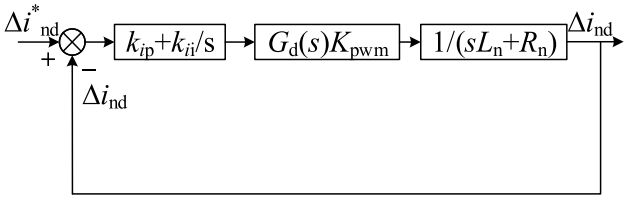

FIGURE 5. Small-signal model of the current inner-loop.

the existing control strategy is a double closed-loop proportional integral control method, combined with dq current decoupling control, the following equation can be obtained as

$$\begin{cases} i_{nd}(s) = \dfrac{(k_{ip} + k_{ii}/s)(i^*_{nd}(s) - i_{nd}(s))G_d(s)}{(sL_n + R_n)} \\ i_{nq}(s) = \dfrac{(k_{ip} + k_{ii}/s)(i^*_{nq}(s) - i_{nq}(s))G_d(s)}{(sL_n + R_n)} \end{cases} \tag{3}$$

where $G_d(s)$ is the system delay link and the small-signal model of the current inner-loop can be plotted as shown in Fig. 5. Since LFO of the coupled system of the traction network rolling stock are analyzed and suppressed by the dd-axis component represented in this paper, only the model of the d-axis current inner-loop is plotted.

Further, combining with power conservation, the input-output power expression can be deduced as

$$\frac{1}{2}(u_{nd}i_{nd} + u_{nq}i_{nq}) = u_{dc}C_d\frac{du_{dc}}{dt} + u_{dc}i_{dc} \tag{4}$$

The physical quantities can be expressed as their corresponding steady-state quantities summed with their small disturbance components, such as

$$\begin{cases} u_{nd} = U_{nd} + \Delta u_{nd} \\ u_{nq} = U_{nq} + \Delta u_{nq} \\ i_{nd} = I_{nd} + \Delta i_{nd} \\ i_{nq} = I_{nq} + \Delta i_{nq} \\ u_{dc} = U_{dc} + \Delta u_{dc} \\ i_{dc} = I_{dc} + \Delta i_{dc} \end{cases} \tag{5}$$

where the upper-case physical quantities in (5) are the steady-state quantities. Combining with (5), (4) can be obtained as follows.

$$\begin{aligned} &\frac{1}{2}(U_{nd}\Delta i_{nd} + \Delta u_{nd}I_{nd} + U_{nq}\Delta i_{nq} + \Delta u_{nq}I_{nq}) \\ &\quad = U_{dc}C_d\frac{d\Delta u_{dc}}{dt} + U_{dc}\Delta i_{dc} + \Delta u_{dc}I_{dc} \end{aligned} \tag{6}$$

Since 4QC of EMUs should ensure the approximate unit power factor operation as much as possible, U_{nq} and I_{nq} can be assumed to be zero. Utilize Laplace transformation, (6) can be expressed as

$$\begin{aligned} \Delta u_{dc}(s) = &\frac{I_{nd}}{2(U_{dc}C_d s + I_{dc})}\Delta u_{nd}(s) \\ &+ \frac{U_{nd}}{2(U_{dc}C_d s + I_{dc})}\Delta i_{nd}(s) \end{aligned}$$

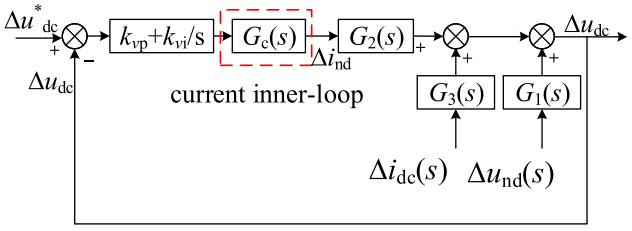

FIGURE 6. Small-signal model of the voltage outer-loop.

$$- \frac{U_{dc}}{U_{dc}C_d s + I_{dc}}\Delta i_{dc}(s) \tag{7}$$

where

$$\begin{cases} G_1(s) = \dfrac{I_{nd}}{2(U_{dc}C_d s + I_{dc})} \\ G_2(s) = \dfrac{U_{nd}}{2(U_{dc}C_d s + I_{dc})} \\ G_3(s) = -\dfrac{U_{dc}}{U_{dc}C_d s + I_{dc}} \end{cases} \tag{8}$$

Combined with (2), the small signal model of 4QC can be drawn as shown in Fig. 6, and the dd-axis input impedance of 4QC can be obtained as

$$Z_{indd} = \frac{\Delta u_{nd}(s)}{\Delta i_{nd}(s)} = \frac{sL_n + R_n + G_4(s) + G_5(s)}{1 - G_6(s)} \tag{9}$$

where

$$\begin{cases} G_4(s) = \dfrac{k_{ip} + k_{ii}/s}{0.5T_d s + 1} \\ G_5(s) = \dfrac{(k_{vp} + k_{vi}/s)(k_{ip} + k_{ii}/s)}{0.5T_d s + 1}G_2(s) \\ G_6(s) = \dfrac{1 + (k_{vp} + k_{vi}/s)(k_{ip} + k_{ii}/s)}{0.5T_d s + 1}G_1(s) \end{cases} \tag{10}$$

As the long-series EMU needs double pantographs (Tp03 and Tp11 or Tp06 and Tp14), single pantograph corresponds to two traction units, and each traction unit can be regarded as two 4QCs in parallel, the total input impedance of the train should be 1/8 times the input impedance of a single 4QC. And because of the need to adopt the impedance matching method to analyze the causes of instability and provide a basis for improvement, the input impedance obtained from the traction converter system combined with the traction transformer is imputed to the network side, the traction transformer ratio is 25000:1900, and the imputed dd-axis input impedance $Z_{in}(s)$ of the EMU can be obtained as

$$Z_{in}(s) = \frac{1}{8}\frac{25000^2}{1900^2}\frac{sL_n + R_n + G_4(s) + G_5(s)}{1 - G_6(s)} \tag{11}$$

C. STABILITY ANALYSIS BASED ON FRC

Based on the principle of impedance matching and FRC, the open-loop transfer function $T_m(s)$ of the coupled system in the worst case (the system structure schematic is shown in Fig. 4) can be expressed as

$$T_m(s) = n\frac{Z_{sdd}(s)}{Z_{in}(s)} \tag{12}$$

TABLE 1. Parameters of coupled system.

Symbol	Quantity	Values
R_s	equivalent resistance of traction network	1.173 Ω
L_s	equivalent inductance of traction network	3.37 mH
u^*_{dc}	reference voltage	2800 V
R_n	equivalent resistance of 4QC	0.0145 Ω
L_n	equivalent inductance of 4QC	3.2 mH
C_d	DC link capacitor	3 mF
k_{vp}	proportional coefficient of voltage controller	0.6
k_{vi}	integral coefficient of voltage controller	2
k_{ip}	proportional coefficient of current controller	1
k_{ii}	integral coefficient of current controller	0.1

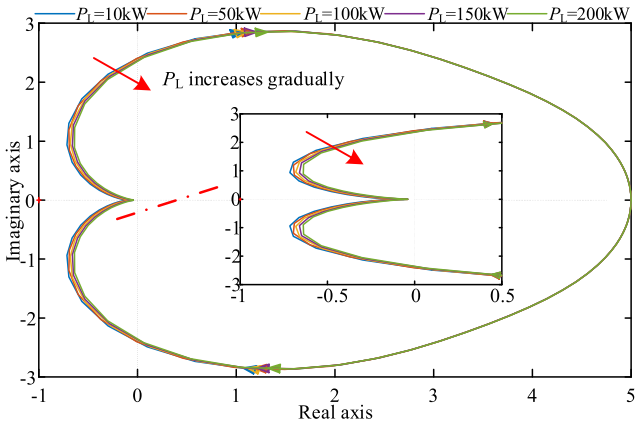

FIGURE 7. Nyquist plots of $T_m(s)$ with different P_L.

Fig. 7 plots the Nyquist curve with various load power when only one EMU operates. The higher the load input power, the more stable the system, which shows that LFO is more likely to occur when the EMU operates under light load. It should be noted that although the stability margin decreases when single EMU begins to operate compared with the full power operation, the system is still stable at this time according to the stability criterion of FRC.

Most of the existing literatures have taken CRH3, CRH5 and other short-series vehicles as the research objects, and proposes that coupled LFO may occur when six or more vehicles start to operate simultaneously. But in existing literature, it is not considered the possible LFO caused by long series EMUs. To further investigate the influence of EMUs number on the system stability, the Nyquist curve of $T_m(s)$ is plotted in Fig. 8. When the number of trains is 3, part of the curve enters the forbidden zone delineated by the red dashed line (the solid part is equal to -1). The system may become unstable at this time. When the number of trains is 2, the system is in a critical stable state.

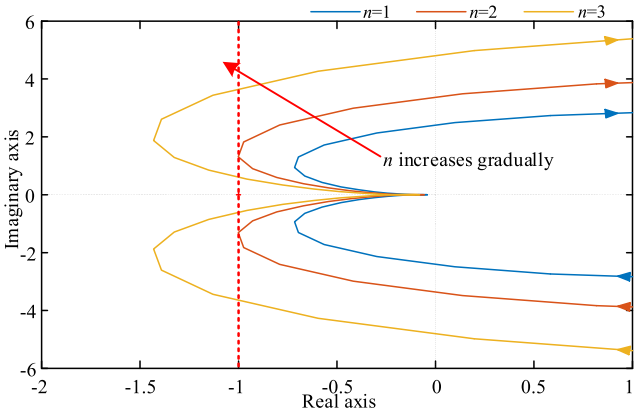

FIGURE 8. Nyquist plots of $T_m(s)$ with different number.

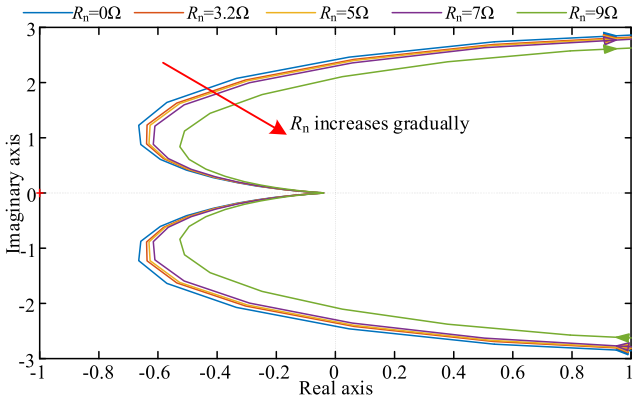

FIGURE 9. Nyquist plots of $T_m(s)$ with different R_n.

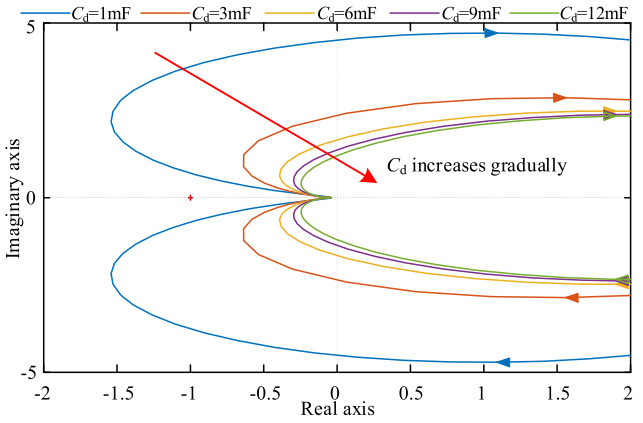

FIGURE 10. Nyquist plots of $T_m(s)$ with different C_d.

To analyze the influence of EMU-side parameters on system stability, the impact of various R_n and C_d of on system stability are analyzed based on Nyquist curves, as shown in Fig. 9 and Fig. 10. It can be seen that the increase of both R_n and C_d will enhance the system stability and improve the system stability margin, where the effect is more apparent when C_d increases. The effect of traction transformer leakage inductance on the stability of coupled system is not analyzed in this paper, please refer to the Appendix for details.

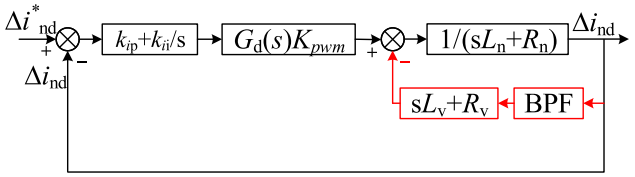

FIGURE 11. Small-signal model of the current with improvement.

Combined with the above analysis, this paper defines the most adverse case for the stability of the coupled system: multiple EMUs operate at the end of the same power supply arm with the condition of rising pantograph. In this case, the existing maximum number of EMUs allowed for stability is two.

IV. VIRTUAL IMPEDANCE WITH BANDPASS FILTER LINK CONTROL STRATEGY

A. MECHANISM OF PROPOSED CONTROL STRATEGY

Although the increase of R_n and C_d will theoretically enhance the system stability, the increase of C_d will affect the actual parameters selection of the second resonant circuit [28]. In addition, there will be errors in the measurement of R_n, which makes it difficult to accurately design parameters. The increase of R_n and C_d will occupy more space, which is not conducive to the lightweight design of EMU.

This paper proposes a virtual impedance with band-pass filtering link control strategy, considering above-mentioned application problems. The small-signal control block diagram of the proposed control strategy is shown in Fig. 11.

In Fig. 11, $(sL_v + R_v)$ is virtual impedance link, BPF represents band-pass Filter, transfer function $G_F(s)$ of which is expressed as

$$G_F(s) = \frac{s/(Q\omega_0)}{(s/\omega_0)^2 + s/(Q\omega_0) + 1} \tag{13}$$

Virtual impedance is used to change the original input impedance of EMU without increasing the actual resistive element and make $T_m(s)$ meet FRC. The band-pass filter link is used to select the specific signal as modified and apply the virtual impedance to the characteristic band of the LFO. It is used to avoid the impact of virtual impedance link on other frequency bands signals, so that the dynamic performance of traction converters can be ensured.

B. DESIGN OF RELEVANT PARAMETERS

The parameters of the band-pass filter need to be designed first such as bandwidth value and center frequency. According to the spectrum of LFO measured in engineering [19], the current harmonics are mainly distributed in 40-60 Hz. So the bandwidth of the band-pass filter link is designed to 20 Hz and the center frequency is set to 50 Hz. Therefore, in (13), ω_0 is set to 314 rad/s and Q is set to 2.5.

Fig. 12 shows the impact of different virtual inductance values on Nyquist curve of $T_m(s)$. k indicates that the virtual resistive value is k times greater than the original resistive value of the system, i.e. $k = (sL_v + R_v) / (sL_n + R_n)$. It is clear that the stability margin of the system gradually increases, as the virtual resistance value increases. When the virtual resistance value equals to the original resistance value, system Nyquist curve meets FRC. However, in order to ensure sufficient stability margin in engineering, the forbidden zone boundary is mostly set to -0.5 in the real part, as shown by the blue dashed line in Fig. 12. To meet the margin requirement in engineering, the virtual resistance value should be selected as three times or more of the existing network side resistance value.

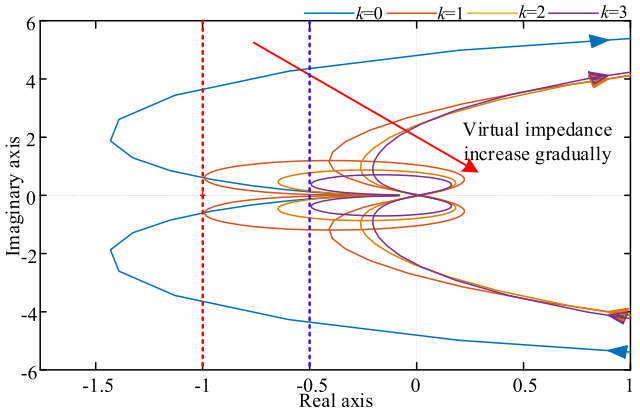

FIGURE 12. Nyquist plots of $T_m(s)$ with different virtual resistance value and inductance value.

Further, Fig. 13 depicts the effect of different virtual impedance values on the voltage bandwidth after setting the parameters of the BPF link. The increase of virtual resistance and virtual inductance will both reduce the system bandwidth, so the increase of virtual resistance and inductance in the time domain system will slow down the system dynamic response process. Therefore, the value of the virtual resistance and inductance can not be too large to ensure system dynamic performance, but should be a compromise between the consideration of system dynamic performance and stability.

In this paper, the principle for the selection of the virtual impedance value is: under the premise of ensuring the system stability margin required in engineering, the smaller virtual impedance value is selected as much as possible to fully ensure the dynamic performance of traction converters. Therefore, the virtual impedance value is selected as three times of the original resistance value, that is, $L_v = 9.6$ mH, $R_v = 0.0435\ \Omega$, and the bandwidth is 46.8951 Hz. With the proposed control strategy, the maximum number of EMUs allowed for stability increases from three to six, as shown in Fig. 14.

V. SIMULATIONS AND EXPERIMENTS

A. SIMULATIONS

To verify the correctness and effectiveness of the proposed control strategy, a simulation platform of the traction network-EMUs coupled system is built in the environment

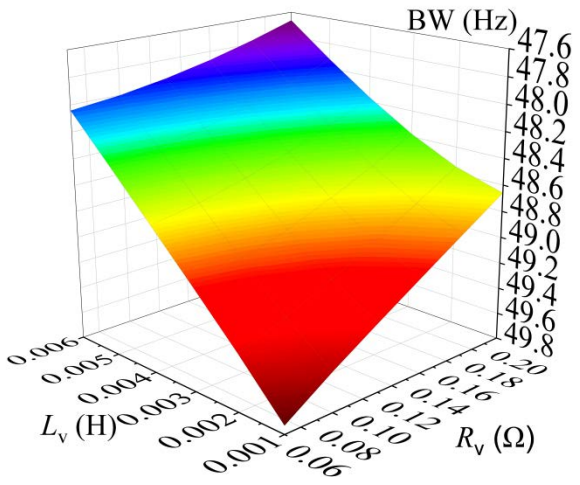

FIGURE 13. The relationship between the bandwidth and different virtual impedance value.

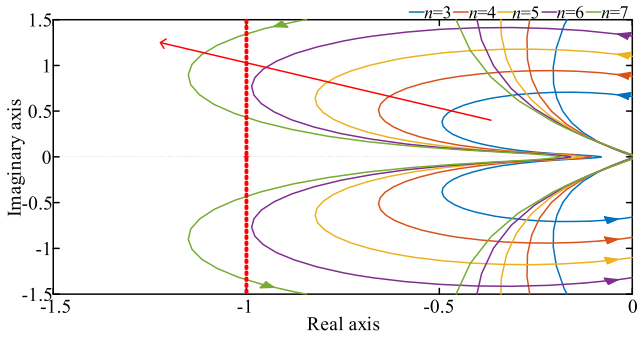

FIGURE 14. Nyquist plots of $T_m(s)$ with different number after adopting proposed control strategy.

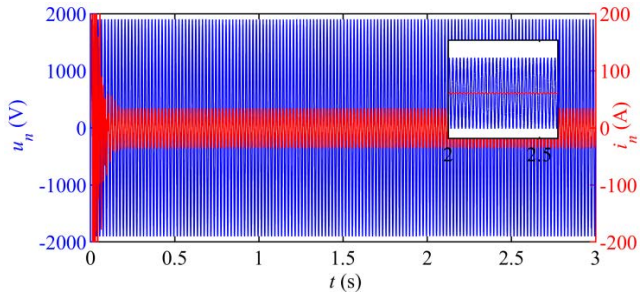

FIGURE 15. Simulation results of u_n and i_n when single EMU operates.

of Matlab/Simulink. Parameters of the traction network and EMU are shown in Table 1.

Fig. 15 verifies that the original control parameters and system electrical parameters proposed in this paper are effective, when single EMU operates. 4QC can work normally and guarantee the approximate unit power factor operation.

Fig. 16 illustrates the waveforms of u_s and i_s when three EMUs operate without improvement. When the number of EMUs is three, LFO occurs and oscillation frequency is about 7 Hz under the worst case scenario. It verifies the

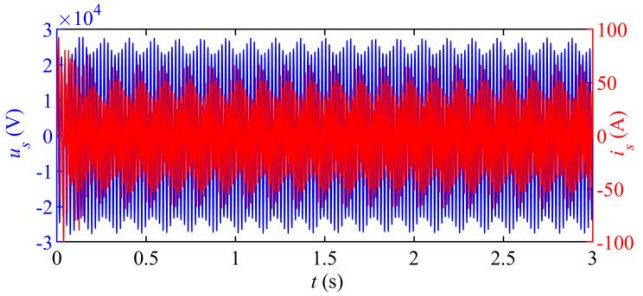

FIGURE 16. Simulation results of u_s and i_s with original control strategy when n = 3.

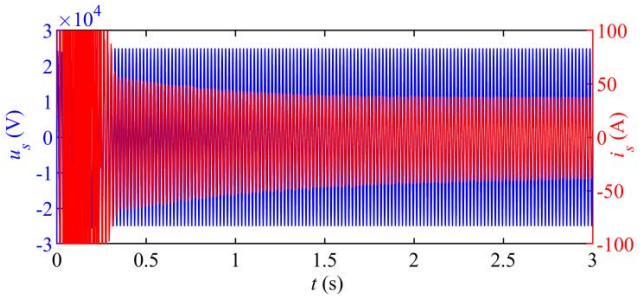

FIGURE 17. Simulation results of u_s and i_s with improvement when n = 3, and k = 2.

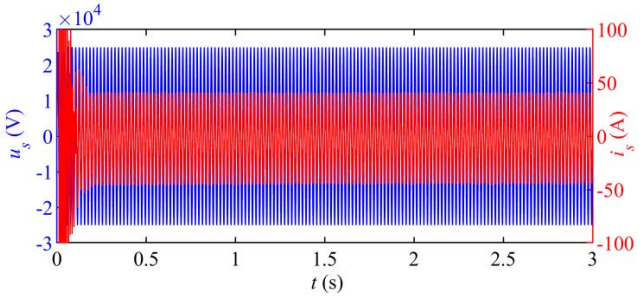

FIGURE 18. Simulation results of u_s and i_s with improvement when n = 3, and k = 3.

conclusion that the simultaneous raising of the three EMUs deteriorates the stability of the network coupling system as described in the previous section.

Fig. 17 shows the the waveforms of u_s and i_s after adopting proposed control when $k = 2$. i_s oscillates at a larger amplitude than u_s in about first 0.2 s, indicating that R_n has a more obvious impact on i_s when LFO occurs under the condition of rising pantograph. After the system starts for 2-2.5 s, the amplitude of i_s gradually decays until it reaches relative stability, which proves that the proposed control strategy in this paper can suppress the low-frequency oscillation, but the suppression effect is limited due to the parameters selection factor at this time.

Fig. 18 depicts the the waveforms of u_s and i_s after adopting proposed control when $k = 3$. At this time the system reaches relative stability after 0.2 s, u_s and i_s do not occur low-frequency oscillations, and the time to reach relative stability is shorter than that in Fig. 17, achieving the desired goal.

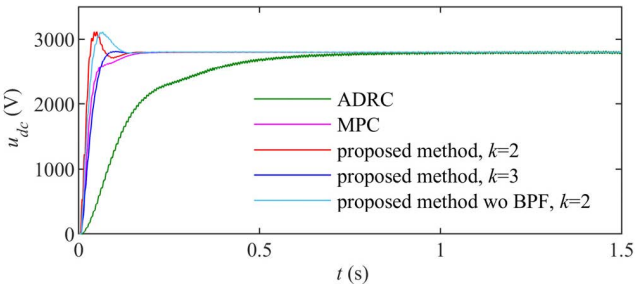

FIGURE 19. Simulation results of u_{dc} with different methods.

TABLE 2. Performance Indexes of Different Methods.

methods	Overshoot(%)	Adjustment Time(s)	Voltage Fluctuation(V)
$k = 2$	3.57	0.23	±2.62
$k = 3$	0.36	0.14	±0.27
wo BPF, $k = 2$	3.56	0.31	±2.80
MPC	none	0.27	±1.48
ADRC	none	0.87	±13.11

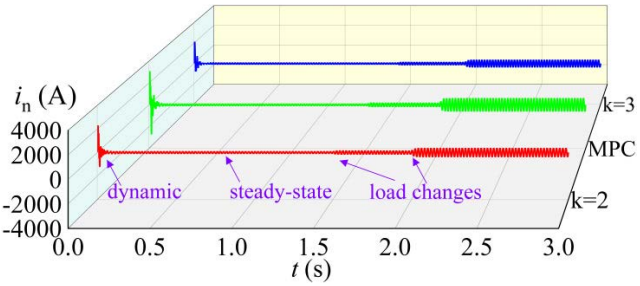

FIGURE 20. Simulation results of i_n with different control strategies.

Further, the proposed method is compared with four different methods, i.e. i) ADRC [24], ii) MPC and iii) virtual impedance control without BPF.

As shown in Fig. 19 and TABLE 2, virtual impedance control strategy has a shorter adjustment time. Dynamic performance of proposed method is better than that of ADRC and MPC. Compared with the condition of $k = 2$, the condition of $k = 3$ takes longer to adjust, but the overshoot is significantly reduced. In addition, the dynamic performance of the method containing BPF is better than that without BPF.

Fig. 20 depicts the waveform of i_n when three different methods are used. Proposed method has the lowest peak current and MPC has the highest peak current. It shows that the proposed control strategy is more suitable for practical application.

The above simulation verifies the effectiveness under the condition of rising pantograph. When EMU eases the braking and gradually starts the loads after the preparation is completed, the simulation analyzes the voltage change of u_{dc} when 4QC adopts the proposed control strategy, as shown in Fig. 21.

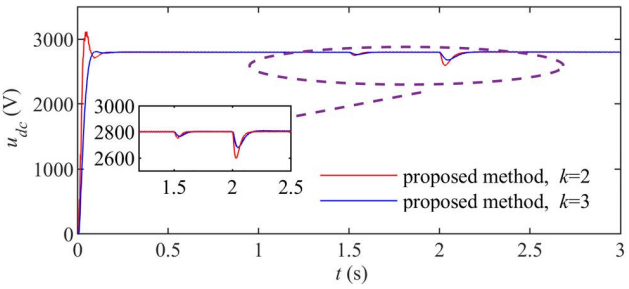

FIGURE 21. Simulation results of u_{dc} with different k when loads operates gradually.

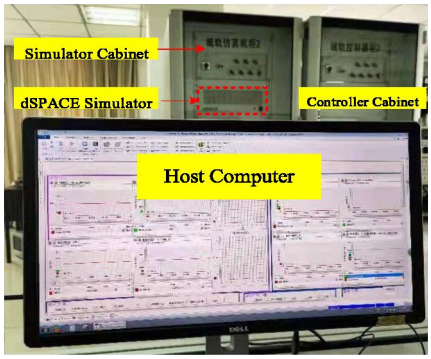

FIGURE 22. Nyquist plots of $T_m(s)$ with different virtual resistance value and inductance value.

At 1.5 s, 225 kW load is put in to simulate the auxiliary converter start-up and the consumption of auxiliary devices. At 2 s, 1200 kW load is applied to simulate the traction inverter unit and traction motors start-up. When the load is applied, the DC link voltage drop decreases with the increase of virtual impedance and the recovery time to the relative stability increases slightly, which verifies that the proposed control strategy can ensure the normal operation of EMU traction mode when $k = 3$.

B. EXPERIMENTS

To further verify the correctness of the theoretical analysis and the proposed control strategy, a simulation model of traction network-EMUs system is built on the hardware-in-the-loop simulation platform. The existing control strategy and proposed control strategy for 4QC are implemented by TI DSP TMS320F28335 control board. The hardware-in-the-loop experimental platform is shown in Fig. 22. u_{pwm} is the input voltage of traction motor; i_{mon} is the input current of traction motor. In this experiment, it is assumed that all EMUs are operating under the condition of rising pantograph.

Fig. 23 shows the waveforms of the system when the original control strategy is adopted and the number of EMUs is three. At this point, the amplitudes of u_n and i_n changes significantly, and oscillation occurs. However, there is no obvious distortion of i_{mon}, indicating that the support capacitance of the existing traction inverters can ensure the normal operation of traction motors when u_{dc} oscillates.

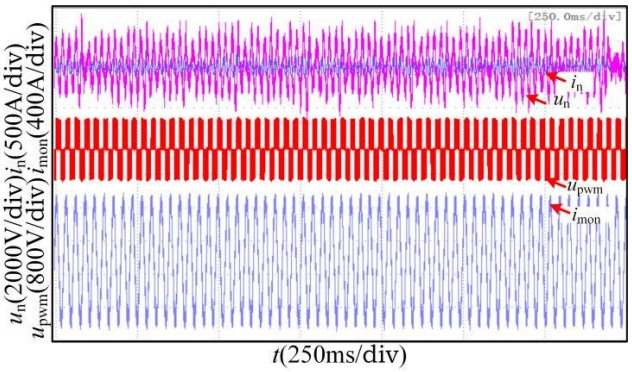

FIGURE 23. Simulation results without proposed control strategy.

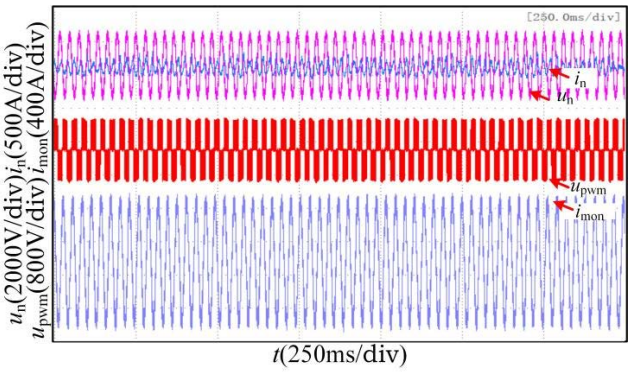

FIGURE 24. Simulation results with proposed strategy when k = 3.

Fig. 24 depicts the waveforms of the system when the proposed control strategy is adopted and $k = 3$. It is clear that the amplitudes of u_n and i_n changes slightly and the oscillation is suppressed. The effectiveness of the proposed control strategy and parameters selection are proved. In addition, the comparison of i_{mon} between Fig. 22 and Fig. 23 shows that i_{mon} does not have obvious distortion, indicating that the proposed control strategy will not affect the normal operation of traction converters.

VI. CONCLUSION

Low-frequency oscillation occurs when three or more EMUs rise pantograph under the worst case scenario. To suppress LFO accidents and ensure dynamic performance of traction converter, a virtual impedance with band-pass filter link control strategy is proposed in this paper. The following conclusions are drawn.

(1) P_L, n, R_n and C_d all affect the coupling system stability. The system stability can be enhanced by increasing P_L, R_n and C_d. Reducing n can enhance the system stability.

(2) Virtual impedance adjusts the input impedance of EMUs equivalently to make $T_m(s)$ meet FRC. The proposed method can improve the system stability margin and suppress the occurrence of LFO in coupled system. The maximum number of EMUs allowed for stability increases.

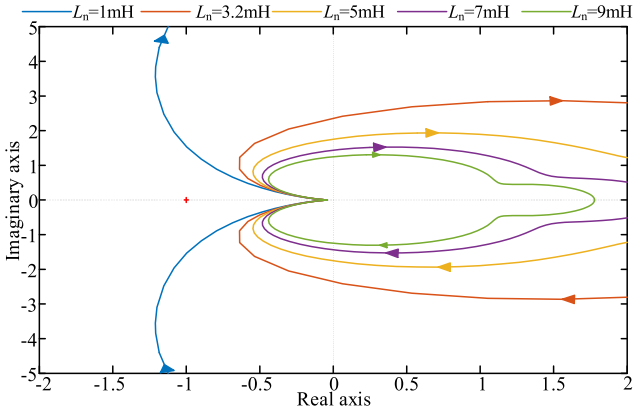

FIGURE 25. Nyquist plots of $T_m(s)$ with different L_n.

(3) The proposed control strategy will increase the magnitude of i_n when EMU starts to operate and decrease system bandwidth. So parameters selection requires a compromise between the stability of the coupled system and the dynamic performance of EMU itself. The proposed control strategy still needs further improvement.

APPENDIX

To analyze the effect of L_n on the coupled system stability, the Nyquist curves of different L_n are depicted, as shown in Fig. 25. With the increase of L_n, system stability margin gradually increases. But according to the existing studies, it cannot yet be qualitatively assumed that the increase of L_n enhances or decreases the coupled system stability [3], [8], [26], [29]-[30]. [29] proposes that the increase of L_n when 4QC adopts instantaneous current control strategy can make the system more stable. [30] proposes that the increase of the equivalent leakage inductance when 4QC adopts dq current decoupling control can make the system more stable, and the same conclusion is not only applicable to the PI controller, but also to the sliding-mode variable structure controller proposed in their paper. The influence of the EMU electrical parameters on the system stability is analyzed by Bode diagram, and the conclusion that the increase of L_n may reduce the system stability is obtained in the literature [8], [26].

According to the conclusions of the above literatures, especially for the comparative analysis of the Bode diagram and Nyquist curve showed in the above literature, it can be seen that the impact of L_n on the coupled system stability may be influenced by the system switching frequency, controller parameters and other electrical parameters at the EMU side. When the EMU-side parameters are different, the trend of the Bode curve may be affected, which in turn will affect the judgment of the impact on the system stability when analyzing different L_n [3] (which can be obtained from a clear comparison of Bode plots in [26], [30]). The impact of different L_n on the coupled system adopting different control and electrical parameters is still to be systematically quantified.

REFERENCES

[1] H. Hu, Y. Zhou, X. Li, and K. Lei, "Low-frequency oscillation in electric railway depot: A comprehensive review," *IEEE Trans. Power Electron.*, vol. 36, no. 1, pp. 295–314, Jan. 2021.

[2] X. Zhu, H. Hu, H. Tao, Z. He, and R. M. Kennel, "Stability prediction and damping enhancement for MVdc railway electrification system," *IEEE Trans. Ind. Appl.*, vol. 55, no. 6, pp. 7683–7698, Nov. 2019.

[3] H. Hu, H. Tao, F. Blaabjerg, X. Wang, Z. He, and S. Gao, "Train–network interactions and stability evaluation in high-speed railways—Part I: Phenomena and modeling," *IEEE Trans. Power Electron.*, vol. 33, no. 6, pp. 4627–4642, Jun. 2018.

[4] Z. Liu, G. Zhang, and Y. Liao, "Stability research of high-speed railway EMUs and traction network cascade system considering impedance matching," *IEEE Trans. Ind. Appl.*, vol. 52, no. 5, pp. 4315–4326, Sep./Oct. 2016.

[5] P. Pan, H. Hu, Z. He, and Y. Li, "Rapid impedance measurement approach based on wideband excitation for single-phase four-quadrant converter of high-speed train," *IEEE Trans. Instrum. Meas.*, vol. 70, pp. 1–11, 2021.

[6] Z. Liu, Z. Geng, and X. Hu, "An approach to suppress low frequency oscillation in the traction network of high-speed railway using passivity-based control," *IEEE Trans. Power Syst.*, vol. 33, no. 4, pp. 3909–3918, Jul. 2018.

[7] X. Lv, X. Wang, Y. Che, and L. Li, "Dynamic phasor modelling and low-frequency oscillation analysis of the single-phase vehicle-grid system," *CSEE J. Power Energy Syst.*, early access, Nov. 20, 2020, doi: 10.17775/CSEEJPES.2020.03160.

[8] K. Jiang, C. Zhang, and X. Ge, "Low-frequency oscillation analysis of the train-grid system based on an improved forbidden-region criterion," *IEEE Trans. Ind. Appl.*, vol. 54, no. 5, pp. 5064–5073, Sep./Oct. 2018.

[9] S. Wu, Z. Liu, Z. Li, H. Zhang, and X. Hu, "Impedance modeling and stability analysis in vehicle-grid system with CHB-STATCOM," *IEEE Trans. Power Syst.*, vol. 35, no. 4, pp. 3026–3039, Jul. 2020.

[10] S. Cheng, L. Ma, X. Ge, L. Peng, and H. Liu, "Low-frequency oscillation analysis in train-traction power supply system using an SISO voltage loop model," *IEEE Trans. Transport. Electrific.*, vol. 8, no. 1, pp. 636–648, Mar. 2022.

[11] H. Wang, W. Mingli, and J. Sun, "Analysis of low-frequency oscillation in electric railways based on small-signal modeling of vehicle-grid system in *dq* frame," *IEEE Trans. Power Electron.*, vol. 30, no. 9, pp. 5318–5330, Sep. 2015.

[12] P. Frutos, J. M. Guerrero, I. Muniategui, I. Vicente, A. Endemano, and F. Briz, "Low-frequency oscillations analysis in AC railway networks using eigenmode identification," in *Proc. IEEE Energy Convers. Congr. Expo. (ECCE)*, Oct. 2021, pp. 1573–1579.

[13] Y. Hong, Z. Shuai, H. Cheng, C. Tu, Y. Li, and Z. J. Shen, "Stability analysis of low-frequency oscillation in train-network system using RLC circuit model," *IEEE Trans. Transport. Electrific.*, vol. 5, no. 2, pp. 502–514, Jun. 2019.

[14] C. Heising, R. Bartelt, M. Oettmeier, V. Staudt, and A. Steimel, "Improvement of low-frequency system stability in 50-Hz railway-power grids by multivariable line-converter control in a distance-variation scenario," in *Proc. Elect. Syst. Aircr., Railway Ship Propuls.*, Oct. 2010, pp. 1–5.

[15] H. Hu, H. Tao, X. Wang, F. Blaabjerg, Z. He, and S. Gao, "Train–network interactions and stability evaluation in high-speed railways—Part II: Influential factors and verifications," *IEEE Trans. Power Electron.*, vol. 33, no. 6, pp. 4643–4659, Jun. 2018.

[16] H. J. Kaleybar, H. M. Kojabadi, M. Brenna, F. Foiadelli, S. S. Fazel, and A. Rasi, "An inclusive study and classification of harmonic phenomena in electric railway systems," in *Proc. IEEE Int. Conf. Environ. Electr. Eng. IEEE Ind. Commercial Power Syst. Eur.*, Jun. 2019, pp. 1–6.

[17] M. A. Azghandi, S. M. Barakati, and A. Yazdani, "Passivity-based design of a fractional-order virtual capacitor for active damping of multiparalleled grid-connected current-source inverters," *IEEE Trans. Power Electron.*, vol. 37, no. 7, pp. 7809–7818, Jul. 2022.

[18] X. Jiang, H. Hu, X. Yang, Z. He, Q. Qian, and P. Tricoli, "Analysis and adaptive mitigation scheme of low-frequency oscillations in AC railway traction power systems," *IEEE Trans. Transport. Electrific.*, vol. 5, no. 3, pp. 715–726, Sep. 2019.

[19] Y. Zhou, H. Hu, X. Yang, J. Yang, Z. He, and S. Gao, "Low frequency oscillation traceability and suppression in railway electrification systems," *IEEE Trans. Ind. Appl.*, vol. 55, no. 6, pp. 7699–7711, Nov. 2019.

[20] S. Wu and Z. Liu, "Low-frequency stability analysis of vehicle-grid system with active power filter based on *dq*-frame impedance," *IEEE Trans. Power Electron.*, vol. 36, no. 8, pp. 9027–9040, Aug. 2021.

[21] D. Lu, Y. Yu, M. Wei, X. Li, H. Hu, and Y. Xing, "Startup control to eliminate inrush current for star-connected cascaded H-bridge STATCOM," *IEEE Trans. Power Electron.*, vol. 37, no. 5, pp. 5995–6008, May 2022.

[22] M. Lapique, S. Pang, J.-P. Martin, S. Pierfederici, M. Weber, and S. Zaim, "Enhanced IDA-PBC applied to a 3-phase PWM-rectifier for stable interfacing between AC and DC microgrids embedded in more electrical aircraft," *IEEE Trans. Ind. Electron.*, early access, Feb. 15, 2022, doi: 10.1109/TIE.2022.3150079.

[23] G. Zhang, Z. Liu, S. Yao, Y. Liao, and C. Xiang, "Suppression of low-frequency oscillation in traction network of high-speed railway based on auto-disturbance rejection control," *IEEE Trans. Transport. Electrific.*, vol. 2, no. 2, pp. 244–255, Jun. 2016.

[24] W. Yu, Z. Liu, and I. A. Tasiu, "Virtual inertia control strategy of traction converter in high-speed railways based on feedback linearization of sliding mode observer," *IEEE Trans. Veh. Technol.*, vol. 70, no. 11, pp. 11390–11403, Nov. 2021.

[25] Z. Shuai, H. Cheng, J. Xu, C. Shen, Y. Hong, and Y. Li, "A notch filter-based active damping control method for low-frequency oscillation suppression in train–network interaction systems," *IEEE J. Emerg. Sel. Topics Power Electron.*, vol. 7, no. 4, pp. 2417–2427, Dec. 2019.

[26] Y. Liao, Z. Liu, G. Zhang, and C. Xiang, "Vehicle-grid system modeling and stability analysis with forbidden region-based criterion," *IEEE Trans. Power Electron.*, vol. 32, no. 5, pp. 3499–3512, May 2017.

[27] R. Burgos, D. Boroyevich, F. Wang, K. Karimi, and G. Francis, "AC stability of high power factor multi-pulse rectifiers," in *Proc. IEEE Energy Convers. Congr. Expo.*, Sep. 2011, pp. 3758–3765.

[28] L. Shen, J. Chen, Z. Jin, Z. Liu, D. Zhou, and C. Wu, "Resonating power decoupling using multifunctional bidirectional DC/DC converter in hybrid railway traction application," *IEEE Trans. Power Electron.*, vol. 37, no. 1, pp. 404–415, Jan. 2022.

[29] R. Deng, B. Liu, and W. Song, "Low-frequency-oscillation analysis and suppression of the coupling system between traction network and multi-locomotives," *Trans. China Electrotech. Soc.*, vol. 34, no. S1, pp. 327–335, Jun. 2019.

[30] S. Yang, Y. Wang, K. Song, M. Wu, and G. Konstantinou, "Stability and suppression study for low-frequency oscillations in network-train system," *IEEE Access*, vol. 8, pp. 30575–30590, 2020.

XUESONG ZHOU received the B.S. degree from the South China University of Technology, Guangzhou, China, in 1984, and the M.S. and Ph.D. degrees from Tsinghua University, Beijing, China, in 1990 and 1993, respectively. From 1993 to 2002, he worked with the School of Electrical and Automation Engineering, Qingdao University, as the Deputy Dean, and the Director of the Shandong Provincial Key Laboratory of Power Electronics Engineering. In 1997, he was promoted to a Full Professor. Since 2002, he has been working with the School of Electrical and Electronics, Tianjin University of Technology, as the Associate Dean, and a Distinguished Professor of the School. His research interests include power system analysis and automation, smart grids, and the field of new energy utilization. In 1996, he won the Guanzhao-Zhi Award from the Chinese Control Industry.

YIFAN HU was born in Hebei, China, 1997. He received the B.S. degree in electrical engineering from the College of Electrical and Information Engineering, Hunan University, Changsha, China, in 2019. He is currently pursuing the M.S. degree in electrical engineering with the Tianjin University of Technology, Tianjin, China. From 2019 to 2020, he was a High-Speed Railway Manufacture Technician with CRRC Tangshan Company Ltd. His research interest includes stability analysis of traction converter systems.

YOUJIE MA received the B.S., M.S., and Ph.D. degrees from Tsinghua University, Beijing, China, in 1987, 1990, and 1993, respectively. From 1993 to 2002, she worked with the School of Electrical and Automation Engineering, Qingdao University. In 1998, she was promoted to a Full Professor. Since 2002, she has been working as a Distinguished Professor with the School of Electrical and Electronic Engineering, Tianjin University of Technology, Tianjin, China. Her research interests include power system analysis and automation and smart grids.

YU TIAN received the B.S. degree from the Hebei University of Science and Technology, Shijiazhuang, China, in 2007. He currently works as the Technical Supervisor of Chinese Standard EMU ''Fuxing,'' CRRC Tangshan Company Ltd. He is also a Senior Engineer. His research interests include troubleshooting of CR400BF and CRH380BL.